A principled approach to polychromatic X-RAY tomography for metal artifact reduction

Shi Yan, Yvain Quéau, Julien Rabin, Jalal M. Fadili

▶ **To cite this version:**

Shi Yan, Yvain Quéau, Julien Rabin, Jalal M. Fadili. A principled approach to polychromatic X-RAY tomography for metal artifact reduction. 2023. hal-04047897

HAL Id: hal-04047897
https://hal.science/hal-04047897v1

Preprint submitted on 27 Mar 2023

HAL is a multi-disciplinary open access archive for the deposit and dissemination of scientific research documents, whether they are published or not. The documents may come from teaching and research institutions in France or abroad, or from public or private research centers.

L'archive ouverte pluridisciplinaire **HAL**, est destinée au dépôt et à la diffusion de documents scientifiques de niveau recherche, publiés ou non, émanant des établissements d'enseignement et de recherche français ou étrangers, des laboratoires publics ou privés.

A PRINCIPLED APPROACH TO POLYCHROMATIC X-RAY TOMOGRAPHY FOR METAL ARTIFACT REDUCTION*

Shi Yan,Yvain Quéau, Julien Rabin, and Jalal Fadili

Normandie Univ, ENSICAEN, UNICAEN, CNRS, GREYC, France

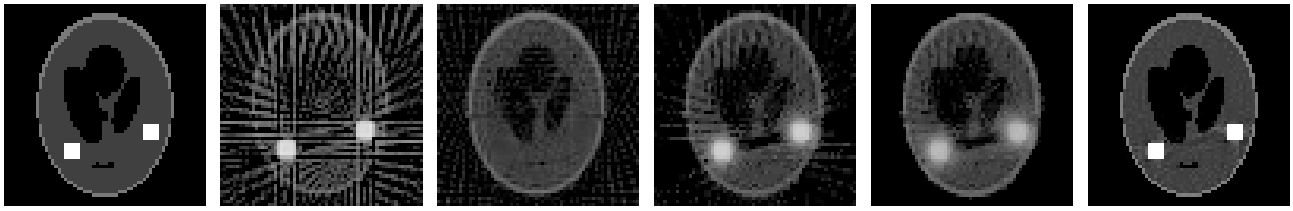

(a) Ground truth (b) FBP (0.71) (c) LI (0.88) (d) TV-ℓ_2 (0.91) (e) TV-KL (0.91) (f) Proposed (**0.99**)

Fig. 1: **Illustration of beam hardening artifacts in CT, when using various methods for reconstruction.** (a) Ground truth image (Shepp–Logan phantom [1]) representing the average polychromatic attenuation coefficients $\bar{\mu}$. Two metallic structures (white squares) are present. (b) Filtered back projection (FBP) [2] gives rise to severe metal streak artifacts. (c) Linear interpolation (LI) [3] does not reconstruct the metal parts. (d,e) Using a monochromatic TV-regularized [4] model with different data fidelity term (ℓ_2 [5] and KL [6]) yields a better reconstruction, though at the price of a loss of contrast. (f) The proposed polychromatic reconstruction is almost artifact-free, and preserves contrast. SSIM Scores are indicated in parentheses (higher is better).

ABSTRACT

We put forward a principled variational approach to computed tomography, in the presence of metals. It is based on the inversion of a forward model accounting both for the polychromatic nature of X-rays, and for the Poisson statistics ruling the photon counting process. A fast and flexible numerical solving framework is proposed, which handles a variety of regularization terms. The efficiency of the proposed method is demonstrated on simulations.

***Index Terms*—** Computed tomography, metal artifacts, variational methods, augmented Lagrangian.

⋆ This work has been funded by Région Normandie under grant ERDF-FSE 2014-2020 no18P03532/18E01765

1. INTRODUCTION

X-ray *computed tomography* (CT) is a noninvasive procedure which uses light ray to image the inside of, *e.g.*, the human body, without damaging it. Unfortunately, the presence of metals *e.g.*, medical implants, may induce severe artifacts in the reconstructed images, as illustrated by Fig. 1. Metal artifacts take the form of dark, bright streaks or cupping, and they occur due to beam hardening, Poisson noise, scattering, and the nonlinear partial volume effect [7]. The objective of the present work is to present a flexible variational framework for metal artifact reduction (MAR) in computed tomography, by taking into account both beam hardening and Poisson noise.

Lambert-Beer law [8, 9] models the attenuation of a light ray as a function of the attenuation coefficients of the materials through which the beam passes. Typically, metals have high density and high atom number, and thus, can absorb more photons than, *e.g.*, water or human tissue [10]. When the X-ray source is monochromatic, all photons have the same energy. Lambert-Beer's law can then be rewritten as a linear system of equations in the unknown attenuation coefficients, which can be solved using established techniques such as filtered back projection [2]. However, X-ray sources have in fact a polychromatic nature [11], which causes the *beam hardening* phenomenon: the mean energy of the beam may be higher after penetrating the object i.e., the X-ray beam is "hardened". This is due to photons with lower energy being more easily absorbed than photons with higher energy, turning the total attenuation coefficient into a nonlinear function of all the attenuation coefficients along the ray. Additionally, the photon counting process is ruled by nonlinear statistics: the number of photons measured by each CT detector approximately follows a *Poisson distribution*. Therefore, low photon counts (which arise, *e.g.*, after crossing metals) will cause higher relative statistical errors [12]. This second nonlinear phenomenon further amplifies metal artifacts in FBP reconstruction (see Fig. 2). In order to limit them, the CT reconstruction process should thus account both for the polychromatic nature of X-rays, and for the Poisson statistics of photon counting. However, the nonlinear inverse problem to solve becomes much more difficult.

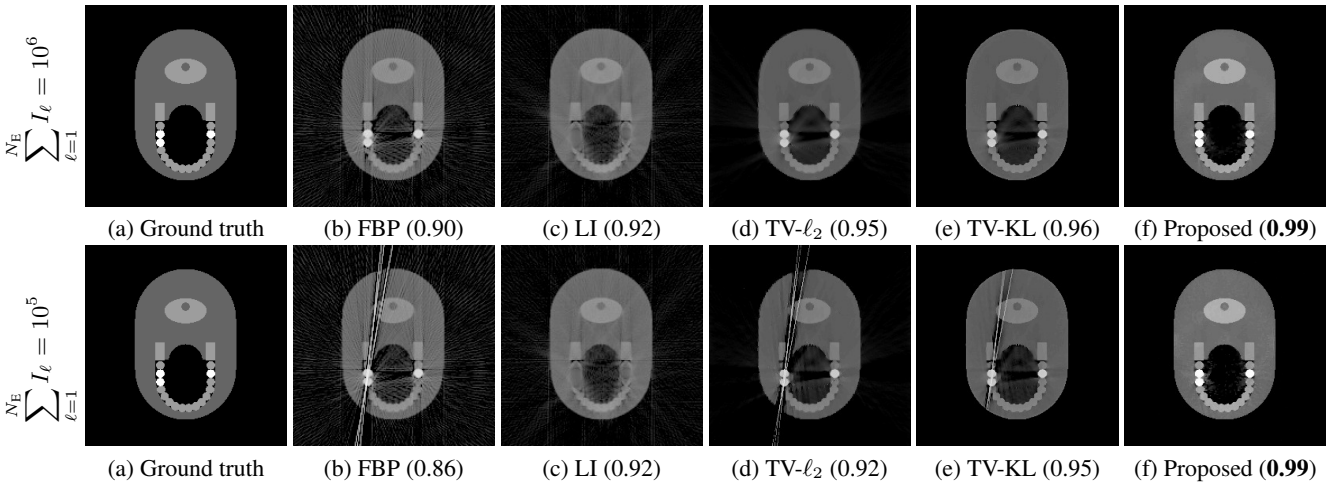

Fig. 2: **Comparison of beam hardening artifacts reduction methods in CT, in normal (first row) or low (second row) photon counts**, with the same notations as in Fig. 1 (displaying the reconstructed average attenuation coefficients $\bar{\mu}$). Low photon counts further amplify metal artifacts in existing CT reconstruction techniques, while the proposed one remains robust even in this challenging setting.

Related works Metal artifacts in CT may be tackled either by improving the design of the scanning system so as to provide polychromatic data, by correcting the obtained sinogram, or by improving the robustness of the algorithmic CT-reconstruction process. Dual energy CT [13] and spectral CT [14] focus on providing a new design of the CT system. Beam hardening correction (BHC) methods [15] aim at correcting the sinogram mismatch between the reality of a polychromatic X-ray source and the assumption of a monochromatic X-ray source. Sinogram correction may also be considered as an interpolation problem, using techniques such as linear interpolation (LI) [3], normalized MAR [16], or frequency split MAR [17]. Yet, these approaches aim at removing the presence of metal from the final image, while such information might be of high interest, *e.g.* for radiation therapy dosimetry. To overcome these shortcomings, MAR reconstruction models such as [18] build upon a proper nonlinear forward model for the attenuation of X-rays, and aim at iteratively solving the inverse problem without modifying the sinogram and preserving the metal. This is also the point of view adapted in our work.

Contributions We present a novel, principled CT-reconstruction method which:

- arises as the natural *maximum a posteriori* (MAP) approach for inverting a forward CT model under Poisson noise and a polychromatic X-ray source;
- is flexible enough to handle a variety of non-smooth regularization terms, *e.g. total variation* (TV) [4];
- combines building blocks from the *alternating direction method of multipliers* (ADMM) [19], *proximal alternating linearized minimization* (PALM) [20] and 0SR1-metric quasi-Newton method [21], resulting in a very fast algorithm;
- is empirically shown to drastically reduce metal artifacts.

2. PROPOSED MODEL

Polychromatic CT consists in recovering the attenuation coefficients $\mu \in \mathbb{R}_+^{N \times N_\mathrm{E}}$, where N is the number of pixels, and N_E is the number of different energy levels at which the object is imaged. To limit the number of unknowns, we assume that this object is composed of N_M known materials, and we denote by $S \in \mathbb{R}^{N_\mathrm{M} \times N_\mathrm{E}}$ the matrix containing the corresponding *mass attenuation coefficients* (expressed in $cm^2.g^{-1}$). This matrix is known, resorting *e.g.* to the NIST database [22]. The unknown attenuation coefficients can thus be considered as a linear combination of the known reference coefficients: $\mu = z\,S$, such that the problem comes down to estimating the unknown densities (in $g.cm^{-3}$) stored in $z \in \mathbb{R}_+^{N \times N_\mathrm{M}}$.

To estimate these densities, we are given a set of N_p noisy observations y_p, $p \in \{1, \dots, N_\mathrm{p}\}$ acquired under different projection angles. We model the sensor responses as random variables Y_p following a Poisson distribution corresponding to the number of actual photons reaching the detector. Combining this with Lambert-Beer law yields the following forward polychromatic CT model, $\forall p \in \{1, \dots, N_\mathrm{p}\}$:

$$Y_p \sim \mathcal{P}\left(r_p \left(\sum_{\ell=1}^{N_\mathrm{E}} I_\ell \exp\left\{-\left(RzS\right)_{p,\ell}\right\}\right) + b_p\right), \quad (1)$$

where $\mathcal{P}$ denotes the Poisson distribution, $r_p \in \mathbb{R}$ and $b_p \in \mathbb{R}$ denote the known gain and background bias on the p-th beam projection angle, I_ℓ denotes the source intensity at energy level ℓ, and $R \in \mathbb{R}^{N_\mathrm{p} \times N}$ denotes the Radon matrix encoding the projective geometry of the CT device.

Resorting to Bayesian inference, the MAP estimate is given by:

$$z^* \in \underset{z \in \mathbb{R}_+^{N \times N_\mathrm{M}}}{\operatorname{argmin}} \; f(z) + \lambda P(z). \quad (2)$$

Therein, the data fidelity term f is constructed from the negative log-likelihood associated with (1):

$$f(z) = \langle b + r \odot e^{-RzS} I, \mathbf{1}_{N_p} \rangle - \langle \log\left(b + r \odot e^{-RzS} I\right), y \rangle, \tag{3}$$

with $\odot$, $e^{\cdot}$ and $\log$ the element-wise multiplication, exponential and logarithm operators, respectively. The regularization term P, on the other hand, stands for some prior knowledge on the solution. In this work we consider, among other things:

$$P(z) = \|\nabla z\|_1 \quad \text{and} \quad P(z) = \|\nabla z S\|_1, \tag{4}$$

where $\nabla : \mathbb{R}^{N \times N_{\mathrm{M}}} \to \mathbb{R}^{2N \times N_{\mathrm{M}}}$ stands for a linear operator approximating the image gradient through finite differences. They correspond, respectively, to anisotropic TV (ATV) regularization [4] on the densities z and on the attenuation coefficients $\mu = zS$. Next, we introduce an efficient algorithm for solving (2).

3. OPTIMIZATION

Incorporating the positivity constraint by means of the indicator function of the positive orthant denoted $h = \iota_{\mathbb{R}_+^{N \times N_m}}$, we first rewrite problem (2) into a generic formulation as

$$\min_z \ \{\Phi(z) = f(z) + h(z) + g \circ A(z)\}, \tag{5}$$

where in the case of ATV regularization, $g(\cdot) = \lambda \|\cdot\|_1$ and $A(z) = \nabla z$ or $A(z) = \nabla z S$. Instead of minimizing $\Phi(z)$ directly, we consider a smoothed version of (5), parameterized by $\beta > 0$:

$$\min_z \ \left\{\Phi_\beta(z) = f(z) + h(z) + {}^{\beta}g \circ A(z)\right\}, \tag{6}$$

where ${}^{\beta}g$ is the Moreau-Yosida envelope of g [23], defined as ${}^{\beta}g(u) = \min_x \ g(x) + \frac{1}{2\beta}\|u - x\|^2$. The argmin is called *the proximity operator* [20] of the function $({}^{\beta}g)$, and it is defined as $\mathrm{prox}_{{}^{\beta}g}(x) = \mathrm{argmin}_u \ g(u) + \frac{1}{2\beta}\|u - x\|^2$.

To solve (6), we introduce an algorithm based on the *alternating direction method of multipliers* (ADMM) [19]. To this end, we consider the augmented Lagrangian $L_{\rho,\beta}(z, u, y)$ associated with (6):

$$L_{\rho,\beta}(z, u, y) = f(z) + h(z) + {}^{\beta}g(u) + \langle y, Az - u \rangle + \frac{\rho}{2}\|Az - u\|^2 \tag{7}$$

where $\rho > 0$. Then, we iterate the following sequence: (z-update) update the primal variable z as the Moreau proximity operator of the linearized augmented Lagrangian at the previous state; (u-update) update the auxiliary variable u by minimizing the augmented Lagrangian; and (y-update) perform a Lagrange multiplier step for y. Using *proximal alternating linearized minimization* (PALM) [20] and the 0SR1-metric quasi-Newton method [21] for acceleration, we eventually obtain Algorithm 1.

Algorithm 1: Optimization of the problem (6)

Initialization: Set parameters β, ϵ and ρ;
Initialize variables $z_{\beta,0}$, $u_{\beta,0}$, $y_{\beta,0}$;
$k \leftarrow 0$.
while $\frac{\|z_{\beta,k+1} - z_{\beta,k}\|}{\|z_{\beta,k}\|} > \epsilon$ **do**

z-update:

$$z_{\beta,k+1} = \underset{z \in \mathbb{R}_+^{N_{\mathrm{M}} \times N_{\mathrm{E}}}}{\mathrm{argmin}} \ \frac{1}{2\gamma_k}\|z - z_{\beta,k}\|^2_{M_k} + \left\langle z - z_{\beta,k}, \partial_z L_{\rho,\beta}(z_{\beta,k}, u_{\beta,k}, y_{\beta,k}) \right\rangle_{M_k^{-1}}.$$

u-update:

$$u_{\beta,k+1} = \frac{\beta}{\rho^{-1}+\beta} X + \frac{\rho^{-1}}{\rho^{-1}+\beta} prox_{(\rho^{-1}+\beta)g}(X), \quad \text{where } X = Az_{\beta,k+1} + \frac{y_{\beta,k}}{\rho}.$$

y-update:

$$y_{\beta,k+1} = y_{\beta,k} + \rho(Az_{\beta,k+1} - u_{\beta,k+1}).$$

$k \leftarrow k + 1$;
end
Result: Primal variable $z_{\beta,k}$ (density of materials)

Therein, γ_k denotes a variable stepsize and M^k a variable preconditioner, with $\langle x, y \rangle_M = x^T M y$ and $\|.\|_M$ the induced metric. Both are set using the 0SR1-metric [21], which yields fast convergence and a closed-form solution for the z-update. The sequence $\{z_{\beta,k}\}_k$ converges to a critical point $z^\star_\beta$ of the smoothed objective function Φ_β as $k \to \infty$, and $z^\star_\beta$ to a critical point of the original objective function Φ, as $\beta \to 0$. The proofs of these claims, detailed in a technical report, are omitted due to space limitation. In practice, one can set $\beta = 0$, which yields a closed-form u-update.

4. EXPERIMENTS

Experimental setting To evaluate our method, we designed a synthetic imaging setup where the sinograms are randomly generated accordingly to Eq. (1), where:

- The ground truth data z is composed of three different homogeneous materials ($N_{\mathrm{M}} = 3$): water, bone and metal, based on the *Shepp–Logan* [1] and the *Jaw* [24] phantoms;
- The spatial resolution is set to 256×256;
- The X-ray source intensity I and the mass attenuation coefficients S are piecewise constant functions defined on N_{E}=*10* equi-width energy intervals $[20, 30], [30, 40] \ldots,$ $[110, 120]$ keV;
- The expected number of photons emitted by the source $\sum_{\ell=1}^{N_{\mathrm{E}}} I_\ell$ is set to 10^6 for all positions and angles;
- The angles defining the discrete Radon transform R are uniformly sampled every $1.5°$ in $[0°, 180°)$ ($N_p = 120$);
- All gains are set to 1: $r_p = 1, \forall p \in N_p$;
- All biases are set to 0: $b_p = 0, \forall p \in N_p$.

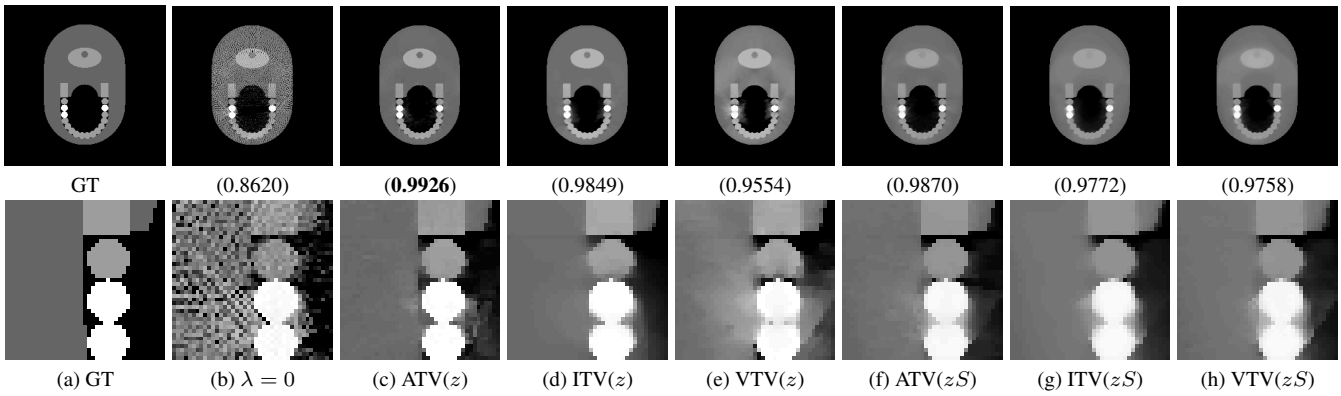

Fig. 3: **Comparison of different regularization strategies for the proposed method.** The first row shows the average attenuation coefficients reconstruction for different settings, along with the SSIM score in parenthesis. The second row shows a close-up view of a dental area where metal implants are present.

Besides, we set $\lambda = 10^3$ for regularization on z and $\lambda = 10^2$ for regularization on zS, $\rho = 10^{11}$ and $\epsilon = 2 \times 10^{-8}$.

Baseline comparison To illustrate the behavior of the proposed method, we carry out in Fig. 1 and the first row of Fig. 2 a comparison with four monochromatic models: FBP, LI, TV-ℓ_2 [5] and TV-KL [6]. To qualitatively compare these results, we display for each method the reconstructed mean attenuation coefficients $\bar{\mu} = \sum_{\ell=1}^{N_\mathrm{E}} \mu_\ell$. To quantitatively assess the quality of the reconstructions, we consider the structural similarity scores (SSIM) [25]. Unsurprisingly, FBP and LI do not successfuly remove beam hardening streaks. Total variation-regularized variational methods, even based on a monochromatic approximation, yield better visual results with much less high frequency artifacts. Notice however that low frequency artifacts remain for TV-ℓ_2 and TV-KL: this results in a noticeable loss of contrast (light grey areas look darker), which means that a post-processing is required to restore the proper scale of the estimated attenuation coefficients if it is used for clinical purpose. On the contrary, the proposed method is almost artifact-free and without loss of contrast. This simple example shows that using a polychromatic model along with an appropriate data fidelity term helps dealing with beam hardening artifacts arising from metal implants.

Low-photon counting experiments Next, we scrutinize the MAR performance of the proposed model for low-photon counting CT. As a result of changing the photon counting of the X-ray emitter, some of the following parameters have been changed accordingly: the expected number of emitted photons is set to $\sum_{\ell=1}^{N_\mathrm{E}} I_\ell = 10^5$, and we further set $\lambda = 100$, $\rho = 10^{10}$ and $\epsilon = 10^{-9}$. The reconstruction results for our approach and other methods are shown in the second row of Fig. 2. We observe how the streak artifacts are now even more striking for most methods, except for the proposed one. For the monochromatic models TV-ℓ_2 and TV-KL, there is again a tradeoff (controlled by λ) between a very regular solution with a large contrast loss and a more faithful result with some strong local artifacts which the SSIM score favors.

Choosing the regularizer To demonstrate the flexibility of the proposed variational framework, we investigate in Fig. 3 the reconstruction result while using other regularization functions. Therein, we compare the results of several variants of total variation: the aforementioned anisotropic TV (ATV), but also isotropic TV (ITV) and vectorial TV (VTV), which are defined in our setting as:

$$P_{\mathrm{ITV}}(z) = \|\nabla z\|_2, \; P_{\mathrm{VTV}}(z) = \sum_{j=1}^{N} \sqrt{\sum_{l=1}^{N_\mathrm{E}} \|\nabla z_{j,l}\|_2}. \quad (8)$$

All these regularization terms can be applied on either the unknown density z or on the attenuation coefficients of the object zS, resulting in 6 different regularization terms: ATV(z), ITV(z), VTV(z), ATV(zS), ITV(zS), VTV(zS). Overall, in these experiments on the *Jaw Phantom*, the anisotropic version of TV is the one which gives the higher SSIM values. Moreover, regularizing the densities z seems to yield slightly better results than regularizing the attenuation coefficients.

5. CONCLUSION

In this paper, we proposed a principled variational approach for metal artefact reduction in X-ray CT. Two major causes of beam hardening and scattering have been taken into consideration in the forward mathematical model: Poisson noise and the polychromatic X-ray source. This model is incorporated into a regularized inverse problem to account for noisy observations. We have then proposed an algorithm based on the augmented Lagrangian framework. The proposed approach is flexible enough to incorporate a variety of regularization terms, and numerical results demonstrate its interest for metal artefact reduction for different scenarios and in comparison of standard techniques. Future extensions of this work will focus on automatic parameter tuning, and combination with deep learning frameworks.

6. REFERENCES

[1] L. A. Shepp and B. F. Logan, "The fourier reconstruction of a head section," *IEEE Transactions on Nuclear Science*, vol. 21, no. 3, pp. 21–43, jun 1974.

[2] P. Kuchment, *The Radon Transform and Medical Imaging*, SIAM, 2014.

[3] W. A. Kalender, R. Hebel, and J. Ebersberger, "Reduction of CT artifacts caused by metallic implants," *Radiology*, vol. 164, no. 2, pp. 576–577, 1987.

[4] L. I. Rudin, S. Osher, and E. Fatemi, "Nonlinear total variation based noise removal algorithms," *Physica D: Nonlinear Phenomena*, vol. 60, no. 1, pp. 259–268, 1992.

[5] Y. Wang, J. Yang, W. Yin, and Y. Zhang, "A new alternating minimization algorithm for total variation image reconstruction," *SIAM Journal on Imaging Sciences*, vol. 1, no. 3, pp. 248–272, 2008.

[6] R. M. Willett, Z. T. Harmany, and R. F. Marcia, "Poisson image reconstruction with total variation regularization," in *IEEE International Conference on Image Processing*, 2010, pp. 4177–4180.

[7] B. De Man, J. Nuyts, P. Dupont, G. Marchel, and P. Suetens, "Metal streak artifacts in X-ray computed tomography: a simulation study," in *IEEE Nuclear Science Symposium and Medical Imaging Conference*, 1998, vol. 3, pp. 1860–1865.

[8] A. Beer, "Bestimmung der absorption des rothen lichts in farbigen flussigkeiten," *Ann. Physik*, vol. 162, pp. 78–88, 1852.

[9] J. H. Lambert, *Lamberts Photometrie (Photometria, sive De mensura et gradibus luminis, colorum et umbrae)(1760)*, Engelmann, W., 1892.

[10] M. A. Haidekker, *Medical Imaging Technology*, Springer, 2013.

[11] H. S. Park, Y. E. Chung, and J. K. Seo, "Computed tomographic beam-hardening artefacts: mathematical characterization and analysis," *Philosophical Transactions of the Royal Society A: Mathematical, Physical and Engineering Sciences*, vol. 373, no. 2043, pp. 20140388, 2015.

[12] J. Hsieh, *Computed tomography: principles, design, artifacts, and recent advances*, SPIE press, 2003.

[13] L. Yu, S. Leng, and C. H. McCollough, "Dual-energy CT–based monochromatic imaging," *American journal of Roentgenology*, vol. 199, no. 5_supplement, pp. S9–S15, 2012.

[14] M. Persson, "Reconstruction of spectral CT images," 2011.

[15] R. A. Brooks and G. Di Chiro, "Beam hardening in x-ray reconstructive tomography," *Physics in medicine & biology*, vol. 21, no. 3, pp. 390, 1976.

[16] E. Meyer, R. Raupach, M. Lell, B. Schmidt, and M. Kachelrieß, "Normalized metal artifact reduction (NMAR) in computed tomography," *Medical Physics*, vol. 37, no. 10, pp. 5482–5493, 2010.

[17] E. Meyer, R. Raupach, M. Lell, B. Schmidt, and M. Kachelrieß, "Frequency split metal artifact reduction (FSMAR) in computed tomography," *Medical Physics*, vol. 39, no. 4, pp. 1904–1916, 2012.

[18] G. Van Gompel, K. Van Slambrouck, M. Defrise, K. J. Batenburg, J. De Mey, J. Sijbers, and J. Nuyts, "Iterative correction of beam hardening artifacts in CT," *Medical physics*, vol. 38, no. S1, pp. S36–S49, 2011.

[19] S. Boyd, N. Parikh, E. Chu, B. Peleato, and J. Eckstein, "Distributed optimization and statistical learning via the alternating direction method of multipliers," *Foundations and Trends® in Machine Learning*, vol. 3, no. 1, pp. 1–122, 2011.

[20] J. Bolte, S. Sabach, and M. Teboulle, "Nonconvex Lagrangian-based optimization: monitoring schemes and global convergence," *Mathematics of Operations Research*, vol. 43, no. 4, pp. 1210–1232, 2018.

[21] S. Becker, J. Fadili, and P. Ochs, "On Quasi-Newton Forward-Backward Splitting: Proximal Calculus and Convergence," *SIAM Journal on Optimization*, vol. 29, no. 4, pp. 2445–2481, 2019.

[22] J. H. Hubbell and S. M. Seltzer, "Tables of X-ray mass attenuation coefficients and mass energy-absorption coefficients 1 keV to 20 MeV for elements Z= 1 to 92 and 48 additional substances of dosimetric interest," Tech. Rep., National Inst. of Standards and Technology-PL, Gaithersburg, MD (United States), 1995.

[23] J. J. Moreau, "Fonctions convexes duales et points proximaux dans un espace hilbertien," *Comptes rendus hebdomadaires des séances de l'Académie des sciences*, vol. 255, pp. 2897–2899, 1962.

[24] "Jaw phantom," http://www.imp.uni-erlangen.de/phantoms/, Accessed: 2021-05-30.

[25] Z. Wang, A. C. Bovik, H. R. Sheikh, and E. P. Simoncelli, "Image quality assessment: from error visibility to structural similarity," *IEEE Transactions on Image Processing*, vol. 13, no. 4, pp. 600–612, 2004.